ACS APPLIED MATERIALS & INTERFACES

Research Article

www.acsami.org

Producing Surfactant-Synthesized Nanomaterials In Situ on a Building Substrate, without Volatile Organic Compounds

Juan F. Illescas and Maria J. Mosquera*

Departamento de Química-Física, Facultad de Ciencias, Universidad de Cádiz, 11510 Puerto Real (Cádiz), Spain

Supporting Information

ABSTRACT: This article describes a sol–gel route for nanomaterials production, without volatile organic compounds (VOCs). These materials are simply obtained by mixing a silica oligomer with a non-ionic surfactant under ultrasonic agitation. The surfactant acts as sol–gel transition catalyst and also as an agent that directs the pore structure of the material, reducing capillary pressure during drying. Thus, a crack-free monolithic material is produced. We also synthesize a novel product with hydrophobic properties by adding OH terminal-polydimethylsiloxane to the starting sol. Importantly, since our synthesis does not require calcination or other additional procedures, the sol can be applied directly onto substrates, particularly the external surface of buildings. Thus, an application of these nanomaterials is to restore and to protect building substrates. Our in-depth investigation of the structure of these materials, using several techniques (physisorption, scanning electron microscopy, transmission electron microscopy, atomic force microscopy, nuclear resonance magnetic spectroscopy), reveals that they are composed of silica particles as a result of the role played by *n*-octylamine. In the hybrid materials, polydimethylsiloxane acts to form bridges linking the silica particles. Finally, we demonstrate the effectiveness of these products for consolidating one particular building stone and making it hydrophobic.

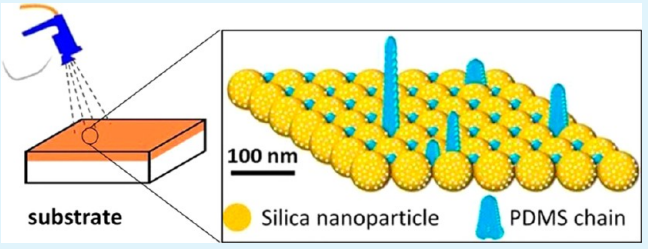

KEYWORDS: *nanomaterial, sol–gel process, PDMS/silica hybrid, structure-directing agent, building materials, consolidants, hydrophobic products*

INTRODUCTION

A well-known drawback of sol–gel materials is their susceptibility to shrinkage and tendency to crack because of the high capillary pressure supported during drying.[1,2] Our research group has previously designed an innovative synthesis strategy in which the sol–gel transition of a tetraethoxysilane monomer (TEOS) occurs in the presence of a surfactant (*n*-octylamine). In this synthesis, HCl is used as a catalyst, water is included in order to hydrolyze ethoxy groups, and ethanol is required as co-solvent.[3] Our target was to design a procedure based on the sol–gel route that could be applied to building stonework or other similar outdoor materials. The surfactant provided an efficient means of preventing cracking of the gel, as the result of two factors: (1) coarsening of the gel network, which reduces the capillary pressure; and (2) decreasing surface tension, which also reduces capillary pressure. Later, we modified this procedure by removing the acid catalyst.[4] We also synthesized crack-free organic–inorganic hybrid gels by co-condensation between an organosiloxane and TEOS in the presence of *n*-octylamine.[4−6] The organic component conferred toughness and flexibility on the product, and collaborated in preventing cracking of the gel; in addition, organic groups were integrated in the silica polymer giving it hydrophobic properties. Recently, we also integrated titania particles in these surfactant-synthesized nanomaterials, thereby obtaining self-cleaning products as a consequence of the photocatalytic activity of titanium dioxide.[7] The practical interest of these low-cost and simple routes has been confirmed, being these materials employed to protect and to restore stones and other building materials. Moreover, other researches working in this field employed later our strategy (*n*-octylamine addition) to obtain crack-free products.[8,9]

The object of the present work is to design a free sol–gel route without volatile organic compounds to produce nanomaterials, in situ, on a substrate. These products are specifically designed for the protection or restoration of building stone or other similar substrate. However, they can be employed for other applications. The novelty of this process regarding to our previous routes is to prevent the employment of ethanol or other organic solvents from the starting sol. There are two important reasons for aiming to remove ethanol and any other volatile organic solvent: (1) to make "green" conservation products and (2) to increase the proportion of dry matter of the product that is applied onto the substrate to improve its effectiveness.

The procedure presented here is based on the route proposed by Tanev and Pinnavaia,[10,11] in which silica precursors, such as TEOS, are assembled around neutral amine surfactant micelles producing a class of hexagonal mesoporous silica (HMS) molecular sieves. The assembly

Received: May 30, 2012
Accepted: July 17, 2012
Published: July 17, 2012

process involved the association of partially-hydrolyzed silica precursors with the surfactant headgroups by hydrogen bonding. In the Pinnavaia route, ethanol was added as co-solvent to improve template solubility. Later, Mercier and Pinnavaia[12] prepared HMS materials by mixing TEOS with *n*-octylamine in an aqueous solution without ethanol as co-solvent. In this preparation, water was added in excess (the molar ratio of TEOS/water is around 1:30). After sol–gel transition, the mesostructure material precipitated and was separated by filtration. For our special requirements (nanomaterials to be produced on the substrate), we cannot add water in excess because phase separation and filtration must be prevented completely. Therefore, we added a proportion of *n*-octylamine aqueous solution capable of being solubilized in the silica precursor, which subsequently prevents phase separation during the sol–gel transition. As surfactant and water content have to be low in order to achieve solubilization, we use a silica oligomer instead silica monomer (TEOS), to accelerate the sol–gel transition and thus, to use a lower surfactant concentration.

In accordance with the preceding, we have developed a simple and low-cost procedure for obtaining crack-free materials that produce, in situ on the substrate, nanomaterials primarily for purposes of stonework restoration and protection. The starting sol exclusively contains a surfactant aqueous solution and a silica oligomer. In addition, we have also developed a simple modification of this process, adding an organic component to the starting sol, to give hydrophobic properties to the final product.

On the other hand, another important achievement of the present work is to carry out in-depth investigation of the structure of the synthesized materials and devise structure models from the experimental data obtained. These models are also used to explain the role played by the different components (surfactant, organic component, ...) in the materials final properties. We also discuss the materials behavior during drying process.

This paper is organized as follows: (1) We present details of the syntheses designed in our laboratory. (2) We carry out a complete characterization of the products obtained and we propose two structure models based on the experimental data obtained. (3) We apply these products onto a stone used commonly in historic building, in a preliminary evaluation of their effectiveness for protection and restoration purposes. For comparison, two commercial products were also evaluated, in all the cases.

EXPERIMENTAL SECTION

Synthesis. Silica nanomaterials were prepared from starting sol containing TES 40 WN (from Wacker) in the presence of a surfactant (*n*-octylamine, from Aldrich). According to its technical data sheet, TES 40 WN (hereafter TES40) is a mixture of monomeric and oligomeric ethoxysilanes. The average chain length is approximately 5 Si–O units. The FTIR spectrum obtained for this product, included as Supporting Information, presentes the peaks typical of an ethoxysilane compound. A second set of experiments was run as a variant on this base sol composition, in which a hydroxyl-terminated polydimethylsiloxane (hereafter PDMS) was added to prepare an organic–inorganic hybrid nanomaterial. PDMS (from ABCR) has a polymerization degree of 12 (molar mass 400–700) and an OH percentage ranging from 4 to 6% w/w. The FTIR spectrum of PDMS, included as Supporting Information, confirmed the presence of terminal Si–OH groups.

The preparation procedure was as follows: (1) an aqueous solution of *n*-octylamine with a concentration of the surfactant significantly higher than that corresponding to its critical micellar concentration (cmc), which is 0.010 mol·dm^{-3},[13] was prepared by vigorous stirring. Specifically, a 1.57 mol·dm^{-3} aqueous solution of *n*-octylamine was employed. Turbidity of solution because of the formation of micelles was clearly observed; (2) the aqueous solution of *n*-octylamine was mixed with TES40 under stirring, in several mole ratios of TES40 to *n*-octylamine ranging from 1:0.1 × 10^{-3} to 1:7.5 × 10^{-3}. Details of the reagent proportions employed are given in Table 1. The sols were homogenized by high-power ultrasonic agitation (60 W·cm^{-3}) for 10 minutes and then cast in cylindrical and transparent molds with dimensions of 3.15 cm diameter and 4.61 cm length. The cast sols were maintained at laboratory conditions (relative humidity of 60% and temperature of 20°C). Those sols producing crack-free monolithic gels were selected in this study. Specifically, the two sols with mole ratios of TES40 to n-octylamine of 1:2.5 × 10^{-4} and 1:5 × 10^{-4} were employed.

Table 1. Properties of TES40/*n*-Octylamine Aqueous Solution Products

water moles[a]	*n*-octylamine moles[b]	gel time (days)	stability (months)	xerogel state
0.003	0.12 × 10^{-3}			no gel
0.006	0.23 × 10^{-3}	5.0	>12	M[c]
0.012	0.46 × 10^{-3}	5.0	>12	M[c]
0.024	0.92 × 10^{-3}	4.0	6.0	C,[d] S[e]
0.036	1.38 × 10^{-3}	3.0	4.5	C,[d] S[e]
0.116	4.43 × 10^{-3}	1.0	4.0	C,[d] S,[e] Y[f]
0.198	7.55 × 10^{-3}	0.5	4.0	C,[d] S,[e] Y[f]

[a]Referenced to 1 mol TES40. [b]Referenced to 1 mol TES40. [c]Monolithic. [d]Cracking. [e]Phase separation. [f]Yellowish coloring.

To prepare organic–inorganic nanomaterials, a second set of sols was synthesized by adding PDMS drop by drop to the sols previously described. To investigate the effect of PDMS content on the properties of the nanomaterials, two different proportions (5 and 10 vol. %) were used. Details of the reagent proportions employed in theses syntheses are given in Table 2. An illustration of the simple synthesis routes designed in this work is shown in Figure 1.

Table 2. Reagent Content of Sols under Study

product	TES40 (% v/v)	PDMS (% v/v)	solution (% v/v)	molar ratio[a]
UCAT-o	99.93		0.075	1: – : 2.3 × 10^{-4}
UCAT-10Po	89.48	10.45	0.075	1: 0.04: 2.5 × 10^{-4}
UCAT-2o	99.85		0.150	1: – : 4.6 × 10^{-4}
UCAT-5P2o	94.30	5.55	0.150	1: 0.02: 4.9 × 10^{-4}
UCAT-10P2o	89.40	10.45	0.150	1: 0.04: 5.2 × 10^{-4}

[a]Molar ratio TES40/PDMS/*n*-octylamine.

Characterization of Nanomaterials. Immediately after the sols had been synthesized, their rheological properties were studied using a concentric cylinder viscosimeter (model DV-II+ with UL/Y adapter) from Brookfield. Experiments were performed at 25°C maintained by the re-circulated water from a thermostatic bath. A shear stress versus shear rate flow curve was generated. For comparative purposes, the rheological properties of two commercial products: Silres BS 290 supplied by Wacker, and Tegovakon V 100 from Evonik (hereafter BS290 and TV100, respectively) were also evaluated. TV100 is a solvent-free one-component consolidant consisting of partially-prepolymerized TEOS and dioctyltin dilaurate (DOTL) catalyst. BS290 is a solvent-free silane/siloxane mix with application as a

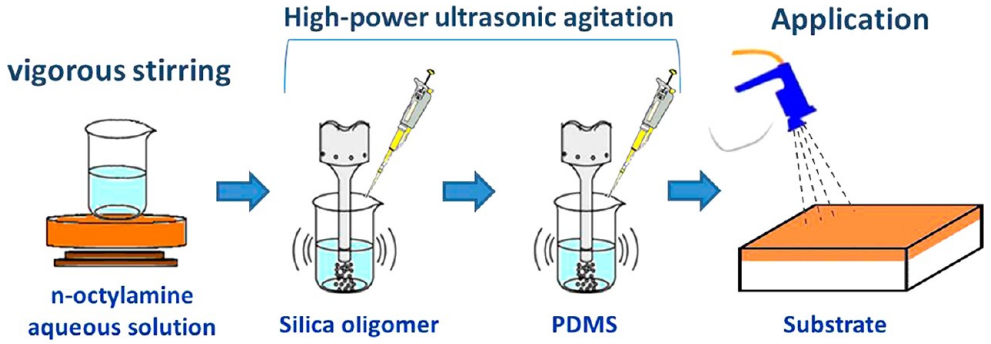

Figure 1. Schematic illustration of the synthesis procedures.

hydrophobic treatment. Following the specifications of the manufacturer, BS290 was diluted in ethanol (dilution = 12% by wt.).

Sols were cast in the molds previously described. Gelation and drying occurred by simple exposure of the cast sols to laboratory conditions (at relative humidity of 60% and temperature of 20°C) until a constant weight is reached. The two commercial products were permitted to gel under the same conditions. The stability of the sols in closed containers was also evaluated by measuring the time taken to gel in the enclosed condition. The presence of cracks in the xerogels was checked by visual inspection. All experiments described below were carried out six months after the synthesis.

The contraction in volume of the materials during drying was calculated from the volume change undergone by the xerogel monoliths, using a digital calliper from Comecta.

The mechanical properties of the xerogels were investigated by applying the Uniaxial Compressive Strength Test on the monoliths obtained. The equipment used was a Shimadzu Autograph AG-I testing machine with a maximum load of 5 KN. The rate of application of the compression load was 0.5 mm/min.

Textural characterization was carried out by N_2 physisorption at 77 K, using a Micromeritics ASAP2020. The isotherms obtained were used to calculate pore volume, pore size distribution and BET surface area of the powdered xerogels.

The surfaces of the xerogels were also visualized by Scanning Electron Microscopy (SEM), using a FEG SEM microscope model Sirion from FEI Company, with a structural resolution of 1.5 nm. Images were captured using a secondary electron detector at a voltage of 10 Kv. Fragments of the materials under study were coated with a thin conducting layer of gold in order to be visualized by SEM.

Transmission electron micrographs from the powdered xerogels were also obtained using high-angle annular dark field-scanning transmission electron microscopy (HAADF-STEM) by means of a JEOL 2010-FEG TEM/STEM electron microscope equipped with a JEOL HAADF detector. For electron microscopy analysis, the samples were prepared by depositing a small amount of the powders directly onto Lacey-Carbon coated Cu grids.

The surface topography of the xerogels surface was investigated using Atomic Force Microscopy (AFM, Nanotec Electrónica S.L.) operated in tapping mode.

The chemical bonds of the nanomaterials under study were analyzed by Fourier Transformer Infrared Spectrophotometry (FTIR). The spectra were recorded in powdered xerogels using a FTIR-8400S from Shimadzu (4 cm^{-1} resolution) in the region from 4000 to 648 cm^{-1}. Experiments were carried out in attenuated total reflection mode (ATR).

Single-pulse (SP) MAS-NMR experiments were carried out on a Bruker AVANCE WB400 spectrometer equipped with a multinuclear probe. Samples of powdered xerogels were packed in 4 mm zirconia rotors and spun at 8 kHz. ^{29}Si MAS NMR spectra were acquired at a frequency of 79.49 MHz, using a pulse width of 1.8 μs ($\pi/2$ pulse length =5.4 μs), a delay time of 60 s and scan number of 2000. The chemical shift values are reported in ppm from tetramethylsilane.

Effectiveness on Stone. The products under study were applied onto a common building stone. The stone selected is a biocalcareous stone from San Cristobal quarry (Cádiz, Spain) that has been employed in emblematic monumental building in Spain's southwest region, such as the Cathedrals of Sevilla and Cádiz. It is a yellow-cream stone composed of about 50% of micritic calcite cement and rounded quartz and feldspar grains, as clastic components. The variety under study had a mercury porosity value of around 21%. The stone samples were cut in the form of cubes of 4 cm sides and dried until constant weight was reached. The sols under study were applied by a spraying process at 1.5 bars during 25 s onto one face of the cube in a similar way as shown in Figure 1. To compare the effectiveness with commercial treatments, BS290 and TV100 were similarly applied. The stone samples were then dried under laboratory conditions until reaching constant weight. Uptake of products and the corresponding proportion of the product remaining in the sample after it is completely dry, which was denoted as dry matter, were calculated. The samples corresponding to untreated stone and their treated counterparts were characterized by the procedures described below, six months after the application. All the results reported correspond to average values obtained from three stone samples consisting of 4 cm-cubes, except when a different number of samples or sample size is expressly indicated.

Improvement in mechanical properties of the treated stone was evaluated using the drilling resistance measurement system (DRMS), by SINT Technology. Drill bits with 4.8 mm diameter were employed with a rotation speed of 600 rpm and penetration rate of 10 mm/min.

The effectiveness of the coating materials in providing hydrophobic protection was characterized by measurement of the contact angle according to the sessile drop method, using a commercial video-based, software-controlled contact angle analyzer, model OCA 15plus, from Dataphysics Instruments. Static contact angle values were determined on the stone surface. For each treatment evaluated, droplets of distilled water (10 μl) were applied by needle to 5 different points on 3 stone surfaces. The advancing and receding contact angles were measured using the ARCA method included in the equipment software, with the volume of the droplet being increased/decreased by 5 μl. Details of this procedure are given in a previous paper.[4]

To confirm the hydrophobic behaviour of the materials, the stone samples were subjected to a test of water absorption by capillarity (WAC) as recommended in UNE-EN 1925[14]

RESULTS AND DISCUSSION

Characterization of Nanomaterials. Sol–gel transition times, stability, and state of the xerogels for the products obtained in our laboratory in the preliminary study are given in Table 1.

As expected, increases of the *n*-octylamine aqueous solution content in the starting sol produced a linear reduction in gel time, demonstrating the catalytic effect played by *n*-octylamine, which we described in previous papers.[3−7] In these previous papers, we explained how the presence of *n*-octylamine clearly modifies the TEOS hydrolysis and condensation processes. In a similar way, stability, which was evaluated as the gel time in

closed vessels, was also reduced as n-octylamine aqueous dissolution content was raised.

As shown in Table 1, the lowest surfactant dissolution content did not gel at laboratory conditions. Thus, this sol was removed from the study because, as previously described, the gel transition must be spontaneous for in situ application. The four sols with the highest surfactant solution content produced cracking xerogels with an evident phase separation, which is a consequence of low solubility between water and TES40. Molar ratio TES40/water equal to or higher than 1/0.024 produced a phase separation and thus, *n*-octylamine, which is held in the aqueous phase, did not interact with the silica oligomer. Consequently, inhibition of the effect of the octylamine in coarsening the pore size gel, which reduces the capillary pressure responsible for cracking, led to the occurrence of gel cracking. Moreover, the two sols with higher surfactant solution content produced yellowish xerogels; this effect could be associated with the higher amine content in the sol producing a silica nitridation.[15,16] Regarding to nitridation process, Han et al.[16] investigated interactions occurred between methylamine and zeolites. They concluded that the strong hydrogen bonding interaction results in the H atom of the amine group attacking the Si−O framework to form Si−O···H···N bond, which leads to the formation of Si−N bonds in the zeolites. We think a similar silica nitridation process could occur in the xerogels prepared in our laboratory.

On the other hand, the yellowish of the xerogels could be interpreted as the amine to carbon dioxide reaction to form carbamate.[17] To clarify this point, we performed the ^{13}C NMR test for the UCA gels under study. As an example, the spectrum corresponding to a UCA product with high octylamine content is included as Supporting Information. As observed, typical signal of carbamate (220 ppm) is not observed. Thus, we think that carbamate is not produced in these materials.

The two TES40/*n*-octylamine sols producing monolithic xerogels (mole ratios of TES40 to *n*-octylamine of $1{:}2.5 \times 10^{-4}$ and $1{:}5 \times 10^{-4}$) were characterized according to the techniques described in the Experimental Section. In addition, we also characterized the properties of the organic-inorganic hybrid nanomaterials prepared in our laboratory. These hybrid materials are denoted by their PDMS and *n*-octylamine contents. All reagent proportions of the sols employed in this study are given in Table 2. The products were named UCA (after University of Cadiz) followed by T (initial letter of TES40) and the letter "o" or "2o" according to the *n*-octylamine proportion. In the case of products containing PDMS, the 5P or 10P suffix was added according to the volume ratio of this component in the starting sol.

For purposes of comparison, the corresponding properties of the two commercial products under study were also investigated. sol−gel properties of the products under study are given in Table 3.

The sols under study exhibited a Newtonian behaviour over the shear range evaluated. Therefore, the viscosity was calculated as the slope of the shear rate versus shear stress curve. In all the cases, the linear regression coefficients were above 0.99. The viscosity of the sols without PDMS synthesized in our laboratory is similar to that of the commercial product TV100. As expected, the addition of PDMS to the starting sol promoted a slight and gradual increase as PDMS content is raised. The commercial hydrophobic product (BS290) showed the lowest viscosity value as a consequence of its dilution in ethanol.

Table 3. Sol−Gel Properties

product	viscosity (mPa·s)	gel time (days)	stability (months)	xerogel state	volume reduction (%)	E^e (MPa)
TV100	4.48	3	2	C[a]		
BS290	3.13			E[b]		
UCAT-o	4.46	5	>12	M[c]	30	135
UCAT-10Po	4.90	2	8	M[c]	37	84
UCAT-2o	4.58	5	>12	M[c]	26	167
UCAT-5P2o	5.04	4	10	M[c]	32	86
UCAT-10P2o	5.35	3	8	M[c]	49	83

[a]Cracking. [b]Evaporated. [c]Monolithic. [e]Elastic modulus.

With regard to the gel times, none of the products gelled instantaneously; this must be avoided for the required applications because, if an instantaneous transition occurs, the product cannot penetrate into the pore structure of the substrate. All of the products gelled spontaneously under laboratory conditions, as required, after lengths of time similar to that taken by the commercial consolidant TV100. The products with PDMS took slightly less time to gel. The explanation for this behavior is that the PDMS chains in the starting sol contain silanol terminals whereas TES40 contains ethoxy groups, which must be hydrolyzed as a prior stage to the gel transition; therefore, the higher the PDMS content in the starting sol, the more rapid the co-condensation process.[6] The presence of silanol terminals in PDMS is confirmed in the FTIR spectrum obtained (see Supporting Information). In the case of BS290, which was applied dissolved in ethanol according to manufacturer's instructions, a thin film was obtained because the solvent was completely evaporated.

All UCA sols showed a significantly longer period of stability than that corresponding to TV100 (at least 4 times longer). This demonstrates that the UCA products have the practical advantage of being stored for considerable lengths of time prior to their application onto substrates requiring treatment.

After it was dried under laboratory conditions, the TV100 sol produced a brittle and completely cracked xerogel, whereas the UCA sols gave homogeneous crack-free and transparent monoliths, as shown in Figure 2.

In the case of the organic-inorganic hybrid xerogels, their homogeneity demonstrates that co-condensation between PDMS and silica oligomers takes place, and that the organic component is fully integrated into the silica gel network. With respect to the reduction in volume undergone by the xerogels during the drying phase, we observed significantly less reduction for these materials than those corresponding to our previously-synthesized products containing a high proportion of water and ethanol as solvents.[4] Specifically, the xerogels prepared with and without PDMS showed reductions of around 83% and 70%, respectively. Our present products, as indicated in Table 3, showed reductions of around 30% and 50%, compared with their corresponding counterparts. Obviously, this significant reduction in volume lost suggests that the resulting dry matter of our products and, consequently, their effectiveness on the substrate treated, has to be greater. As expected, the volume reduction for the monolithic materials was greater for those containing PDMS, and increased as PDMS content is raised. As Mackenzie et al. discussed,[18] PDMS chains react initially to the stress produced during

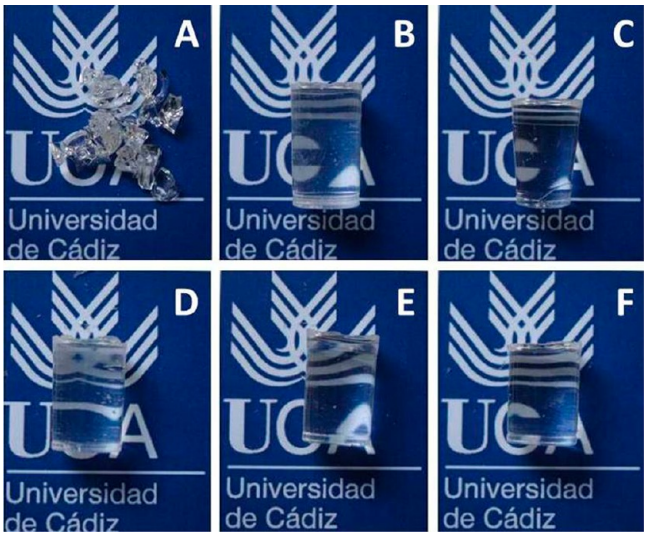

Figure 2. Photographs of xerogels: (A) TV100, (B) UCAT-o, (C) UCAT-10Po, (D) UCAT-2o, (E) UCAT-5P2o, and (F) UCAT-10P2o.

drying by coiling up, thus producing a greater reduction in volume of the material. In order to check this behavior, elastic modulus (E) values were obtained from the stress-strain test for the monolithic xerogels (see Table 3). As expected, the elastic moduli were lower for the xerogels containing PDMS, confirming its "rubbery" behavior.

Textural properties of the xerogels were determined from nitrogen adsorption−desorption experiments. The commercial product TV100 cannot be evaluated because of its extremely low pore volume, which was not detected by the equipment. This feature confirms that the xerogel obtained from TV100 is a dense microporous material. Nitrogen adsorption-desorption isotherms corresponding to the gels prepared in our laboratory are shown in Figure 3 (top), and the textural data obtained are given in Table 4.

All of the UCA materials showed type IV isotherms, which are typical of mesoporous materials, according to the IUPAC classification. However, some differences between products with PDMS and their corresponding counterparts are observed. The two products without PDMS (UCAT-o and UCAT-2o) presented a H1 hysteresis loop with nearly parallel and vertical adsorption−desorption branches, this phenomenon being more obvious in the product with the lowest *n*-octylamine content. This hysteresis is typical of materials consisting of spherical particles arranged in a fairly uniform way.[19] The UCA products with PDMS showed a type H2 hysteresis loop, characterized by a triangular shape and a steep desorption branch, which suggests that connectivity between pores is lower than that corresponding to the H1 type. Since the desorption branch was found to be located at relative pressures close to a lower pressure limit (about 0.4 for N_2 at 77 K), these xerogels can be also classified as materials with relatively uniform channellike pores.[19,20]

Figure 3 (bottom) shows the pore size distribution obtained by the Barret−Joyner−Halenda (BJH) method from the isotherm desorption branches.[21] In a previous paper, Tanev and Pinnavaia[10] synthesized mesoporous silica using different non-ionic surfactants (including n-octylamine) as template for the pores of the materials. These hexagonal mesoporous molecular sieves showed two clearly differentiated degrees of

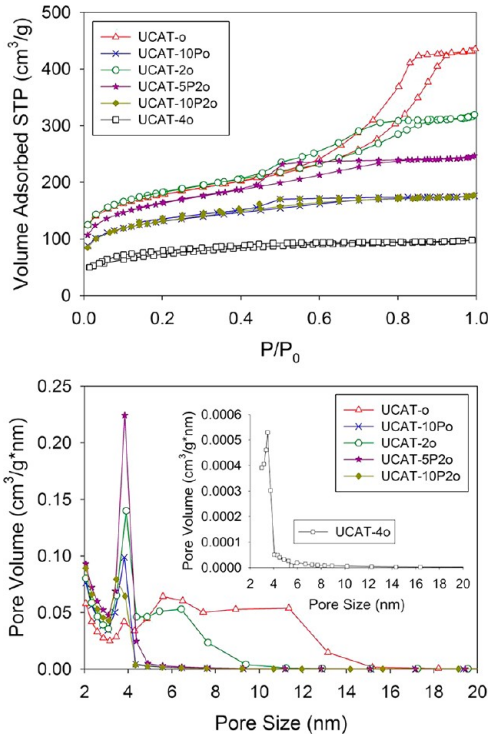

Figure 3. Nitrogen isotherms (top) and BJH pore size distribution (bottom) for the nanomaterials under study.

Table 4. Textural Parameters for the Nanomaterials under Study

product	total pore volume (cm^3/g)	pore size (nm)	BET surface area (m^2/g)	particle size (nm)
UCAT-o	0.67	3.81/5.59	618	111
UCAT-10Po	0.27	3.82	456	71
UCAT-2o	0.49	3.91/6.43	634	125
UCAT-5P2o	0.38	3.84	571	67
UCAT-10P2o	0.27	3.45	460	56
UCAT-4o	0.15	3.48/5.94	264	---

mesoporosity: (1) framework-confined mesoporosity, which is the porosity created by the surfactant, characterized by nitrogen adsorption centred on relative pressures (P/P_0) ranging from 0.1 to 0.5 in the isotherms; and (2) textural mesoporosity, which is the interparticulate porosity, characterized by the appearance of a well-defined hysteresis loop in the P/P_0 region from 0.5 to 1.0 in the corresponding isotherms. These two kinds of mesoporosity were clearly identified in the UCA products without PDMS, in which a homogeneous distribution centred on 3.8−3.9 nm, corresponding to pores created by the *n*-octylamine, is observed. In addition, a coarser and heterogeneous pore size distribution is located in the region from 5 to 14 nm. This latter distribution could be associated with interparticulate spaces inside the gel network. In the UCA products with PDMS, the lowest mesoporosity values are maintained, with size and homogeneity values similar to those observed for gels without PDMS. This finding demonstrates the role played by *n*-octylamine as pore-directing agent. However, porosity associated with interparticulate spaces is completely absent from all the UCA products with PDMS, and we think this is a consequence of the high shrinkage suffered by

PDMS chains during the gel drying phase. This hypothesis is supported by the lower elastic modulus values obtained and greater reduction in volume undergone by the xerogels with PDMS.

In order to explain the cracking observed for xerogels synthesized with higher n-octylamine content, we carried out a physisorption test in the xerogel containing a TES40/*n*-octylamine molar ratio of 1:0.9 × 10^{-3}. This xerogel, which presented phase separation and cracking during drying (see Table 1), was denoted UCAT-4o. The pore volume of this xerogel was significantly lower than those obtained for the other UCA gels tested (Figure 3 and Table 4). With regard to its pore size distribution, we clearly observe that the mesoporosity created by the *n*-octylamine is maintained but its pore volume is extremely low. These results confirm our hypothesis that the increased content of *n*-octylamine aqueous solution in the starting sol promotes a phase separation; consequently, *n*-octylamine acts only weakly in directing the material pore structure, and so the proportion of mesoporosity created is significantly lower. Subsequently, capillary pressure is maintained at a high value during the xerogel drying and cracking occurs.

We also visualized the surfaces of the xerogels under study by SEM. The images obtained are shown in Figure 4. This study

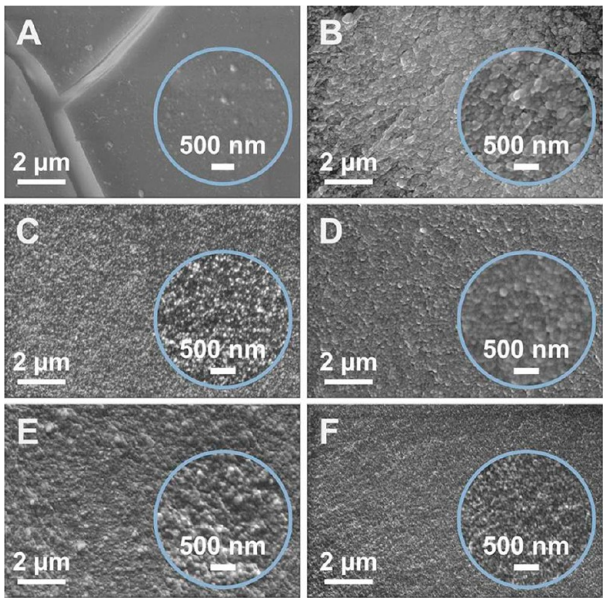

Figure 4. SEM images of the xerogels under study at 20000× magnification: (A) TV100, (B) UCAT-o, (C) UCAT-10Po, (D) UCAT-2o, (E) UCAT-5P2o, and (F) UCAT-10P2o.

provided evidence supporting that obtained from the nitrogen adsorption tests. As shown in Figure 4A, the xerogel from TV100 is a dense material in which pores are not observed at the magnification used. Cracks can be clearly observed in the left side of the picture. In the case of UCA products (Figures 4B–F), all of them consist of a configuration of silica particles of nearly uniform size. In a previous paper,[5] we obtained a similar structure for xerogels synthesized from TEOS, PDMS and *n*-octylamine, using water and ethanol as solvents. Xerogels with similar structures have widely been reported in the literature. In particular, Orcel et al.[22] also obtained a gel network composed of silica balls from sols containing tetramethoxysilane and formamide. They proposed a mechanism for the sol–gel transition in which primary particles of around 2 nm are aggregated in secondary particles of about 6 nm. Gelation occurred when these secondary units agglomerate with each other and formed a three-dimensional network. In a similar way, Bogush and Zukoski[23] obtained uniform spheres ranging from 50 nm to over one micrometer in diameter, from TEOS in aqueous ethanol solution containing ammonia. These authors[24] developed an aggregative growth model to explain the formation of these uniform silica particles in a presence of a basic medium, such as ammonia, in which the rate of condensation is faster than the hydrolysis. More recently, Kosuge and Singh[25] also synthesized materials composed of mesoporous particles by using *n*-octylamine as template. We speculate that the formation of uniform silica particles in our products occurs by a similar aggregation mechanism. We think *n*-octylamine acts as a basic catalyst, promoting the condensation of silica oligomers present in the starting sol.

Recently, Zhang et al.[26] employed Zukoski's aggregation model to explain the hybrid organic–inorganic gels structures produced from TEOS and PDMS. They concluded that a network of silica particles is formed by the aggregation of silica reactive species from TEOS, in which PDMS chains create bridges between particles. Previous structural studies of these hybrid materials by small angle X-ray scattering also described them as PDMS chains crosslinked by silica based particles.[27] Moreover, PDMS could also form coatings on the particles surface, as is also proposed by Zhang et al.[26]

The SEM images obtained in our laboratory (see Figure 4) clearly show that the nanomaterials with PDMS are composed of a configuration of silica particles with lower size and smaller interparticulate distance than those corresponding to materials without PDMS. We measured the size of these particles from SEM images and the data obtained are given in Table 4. The two products containing PDMS show a particle size ranging from 50 to 70 nm, which is reduced as the organic content is raised. In the case of the nanomaterial without PDMS, the particles size is significantly higher, at around 110–120 nm.

These findings were supported by the transmission electron micrographs. Figure 5 shows micrographs corresponding to a material without PDMS (UCAT-2o) and its counterpart with PDMS (UCAT-10P2o). The HAADF-STEM micrograph of UCAT-2o shows an individual silica particle from its gel network with a size similar to that estimated by SEM (around 100 nm). In the case of the hybrid material containing PDMS, we observed a smaller particle size (around 70 nm), which again matched the size estimated by SEM.

In our view, the reduction in size and distance between particles found for the hybrid xerogel networks is associated with the shrinkage of PDMS bridges during xerogel drying as a consequence of their high elasticity.[18] As previously discussed, the modulus of elasticity is expected to be very low because the primary reaction to the stress is the coiling up of the PDMS chains. This is also confirmed by the increased degree of material shrinkage (% volume reduction) and the bulk modulus increase presented by the nanomaterials with PDMS (see Table 3). This reduction in size could be also favored by the formation of hydrophobic PDMS coatings on the silica particles which could restrict further aggregations.

Figure 6 shows a 2D structure model for the hybrid materials containing PDMS and for their counterparts without PDMS, obtained in accordance with the previous discussion.

We also investigated by AFM the surface topography of the UCA xerogels. Figure 7 shows the 3D images obtained. It

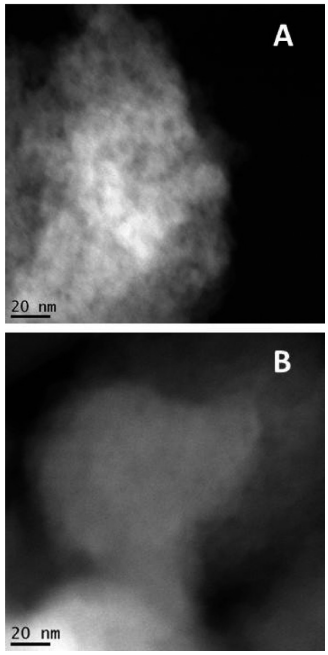

Figure 5. HAADF-STEM images of (A) UCAT-2o and (B) UCAT-10P2o.

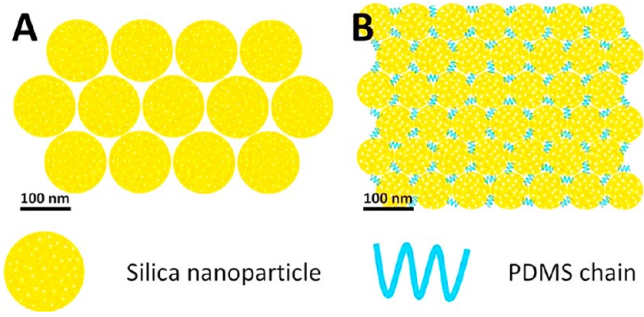

Figure 6. 2D structure model for (A) silica nanomaterials and (B) silica–PDMS nanomaterials.

should be noted that the *z*-axis has been significantly enlarged with respect to the *x* and *y* axes. This was done in order to make the difference in roughness of the different materials under study easier to observe.

To investigate the effect of PDMS on their topography, we also prepared a nanomaterial with higher PDMS content (50% v/v). It was denoted UCAT-50P2o. Its 3D image is also included in Figure 7.

Surfaces of the silica nanomaterials without PDMS presented a slight roughness, which we associate with the aggregation of the silica particles. Addition of PDMS substantially modified the surface morphology of the nanomaterials: peaks appear that greatly increase their surface roughness. As we discussed previously, these peaks may be associated with the PDMS chains,[6] and this is corroborated by the clear linear trend toward more peaks with higher PDMS content, as shown in images 7D, 7E, and 7F. These results clearly confirm our previous discussion about the xerogels' structure. PDMS aggregates, which form bridges linking silica particles, contract shrink significantly during their drying phase, as previously reported in this study. This results in the contraction of the bridges, giving rise to the roughness peaks shown in the AFM 3D images. In accordance with this hypothesis, we develop one

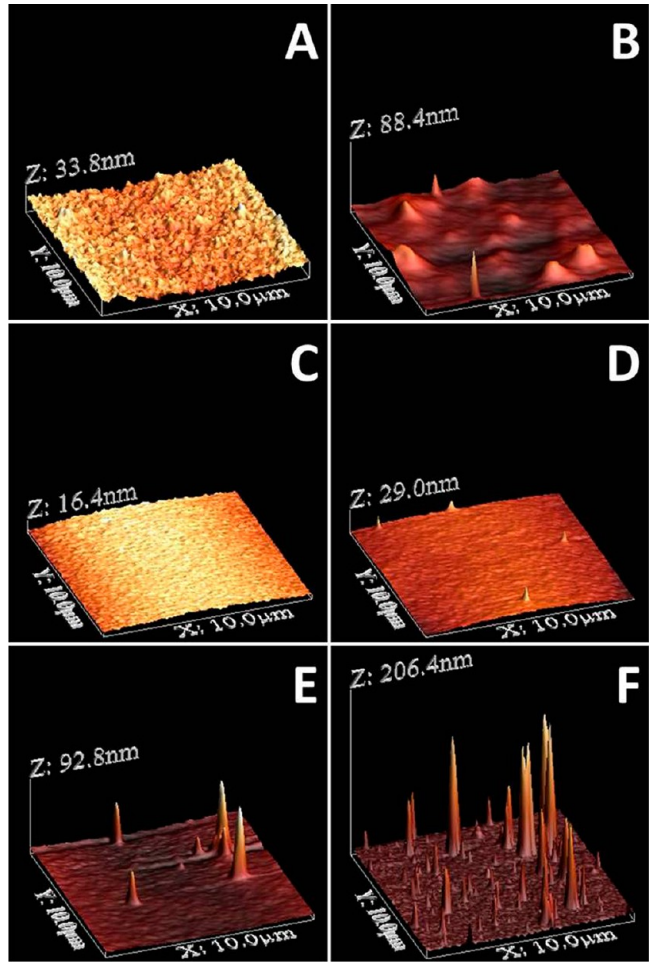

Figure 7. AFM 3D topography images of the nanomaterials' surface. (A) UCAT-o, (B) UCAT-10Po, (C) UCAT-2o, (D) UCAT-5P2o, (E) UCAT-10P2o, and (F) UCAT-50P2o.

3D model for the hybrid silica PDMS structure and another for its counterpart without PDMS, from the AFM images obtained. The two 3D models are shown in Figure 8.

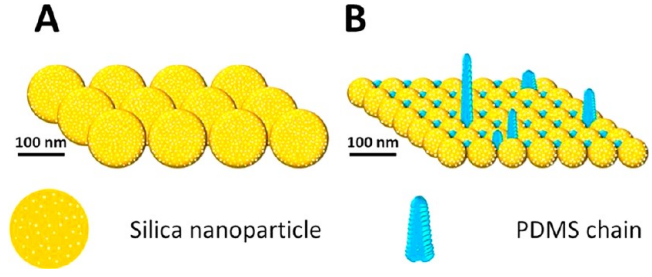

Figure 8. 3D structure model for (A) silica nanomaterials, and (B) silica–PDMS nanomaterials.

FTIR spectra of the nanomaterials under study are presented in Figure 9. All the materials, including the commercial products, presented two peaks typical of siloxanes, located at 792 and 1043 cm^{-1}, corresponding to bending and stretching vibrations, respectively.[3,28] UCA xerogels also showed a peak adjacent to the stretching vibration, located at 1161 cm^{-1}. This double band (1043–1161 cm^{-1}) is associated with chains of high-molecular weight siloxanes.[29] In the case of the TV100 product, this additional band was not observed and

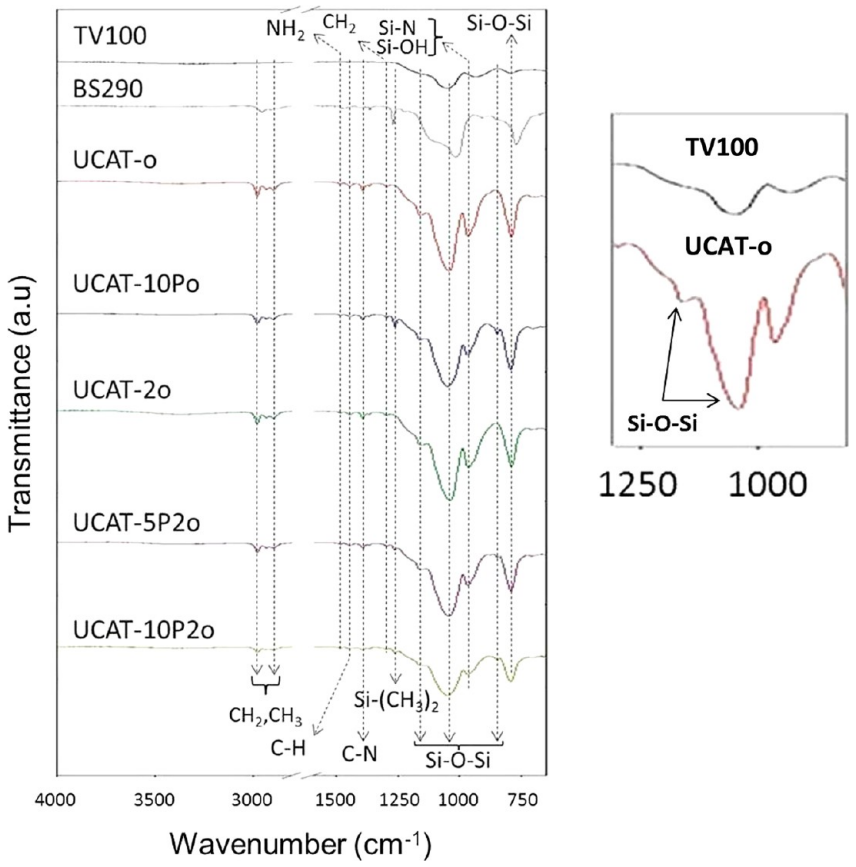

Figure 9. FTIR spectra of the nanomaterials under study.

subsequently, a lower molecular weight polymer could have been formed. An enlargement of the region of the FTIR spectrum corresponding to this double bond has been included in Figure 9.

Specific peaks attributed to PDMS were observed in the UCA hybrid materials and BS290 product. In particular, the peak at 1261 cm^{-1}, attributed to the Si-$(CH_3)_2$ bond,[26,28] is clearly shown in these spectra; UCA products also show the band at 860 cm^{-1} assigned to the copolymerization reaction between Si−OH groups of hydrolyzed silica oligomers and Si−O groups of PDMS molecules.[28] As suggested by Zhang et al.,[26] these hybrid materials were exhaustively extracted with ethanol using a Soxhlet apparatus to remove PDMS not bonded to the silica, with all the bands reported here being maintained after extraction. This showed that PDMS is covalently bonded to silica particles, confirming that the copolymerization of PDMS and silica oligomers is effective. Obviously, these bands are not observed in the spectra for UCA materials without PDMS and TV100.

We observed the presence of n-octylamine in the xerogels tested. Specifically, the bands at 1392 and 1444 cm^{-1}, appearing exclusively in UCA products, are attributed to *n*-octylamine C−N stretching[3,30] and *n*-octylamine C−H bending,[4,30] respectively. In addition, we observe a peak at 1485 cm^{-1} which, according to the literature,[31] results from amino groups strongly hydrogen-bonded to free silanols. This confirms that the n-octylamine interactions and the silica precursor are produced by hydrogen bonds.

The peak at 970 cm^{-1} shown in the spectra of UCA products deserves particular attention. It can be attributed a priori to Si−OH stretching vibration.[3] However, its intensity does not decrease in hybrid products containing PDMS. Moreover, the typical broad band shown for silica gels at 3750-3250 cm^{-1} associated with hydrogen-bonded silanol groups with absorbed molecular water is not shown in these spectra.[3] Consequently, we think that the 970 cm^{-1} peak could be attributed to Si−N stretching vibration.[32] This might be confirmed by the yellowish coloring observed for the products prepared in the previous study, described in this paper, with higher *n*-octylamine content associated with a silica nitration[15,16] (see Table 1).

On the other hand, we earlier synthesized nanomaterials from TEOS, water and ethanol in the presence of *n*-octylamine.[3] We demonstrated that the surfactant was completely removed after 6 months. We think that the removal of surfactant was facilitated by the excess of ethanol content in the sol (ranging from 4 to 22 mols for 1 TEOS mol), since ethanol, with n-octylamine residues, was evaporated during drying. In the products presented here, evaporation is significantly lower as demonstrated by the smaller reduction in the xerogel volume. Thus, n-octylamine could be partially retained in the xerogels obtained as observed in the spectra.

We also observed a band related to the asymmetric vibration of the $-CH_2-$ group at 2922 cm^{-1} and to the symmetric vibration of the CH_3- and $-CH_2-$ groups at 2852 cm^{-1}, in the case of alkyl chains.[29] These two bands are clearly observed in all the UCA products. A single band in an intermediate position between the two cited bands was also observed in BS290. In BS290, we think this band corresponds to the alkyl groups included in this commercial product, giving hydrophobic properties. In the UCA products, these peaks could be associated with the surfactant because they are present, at the

same intensity, in the spectra of silica xerogels and silica–PDMS xerogels. However, they could also correspond to ethoxy groups from non-hydrolyzed oligomers. In the UCA materials, we also observe a band at 1296 cm^{-1}, corresponding to CH_2 twist vibration, which could be also attributed to ethoxy groups.[33] The spectrum of TV100 did not show these bands.

The ^{29}Si NMR spectra for all the xerogels obtained are shown in Figure 10. The TV100 spectrum showed Q_3 (−100 ppm) and Q_4 (−110 ppm) species with a similar intensity. In the case of the UCA nanomaterials, we also observed Q_4 and Q_3 species. In these materials (except UCAT-o), the Q_4 peak, attributable to tetrafunctional buildings, is higher than that corresponding to Q_3, indicating a more cross-linked framework due the effect of n-octylamine. This higher degree of reticulation is typical of silica species condensed as particles.[34] It was also observed in silica particle mesostructures obtained by using amine surfactants as a template.[11] This feature confirms that n-octylamine produces nanomaterials composed of a network of silica particles, as was visualized by SEM and TEM (see Figures 4 and 5).

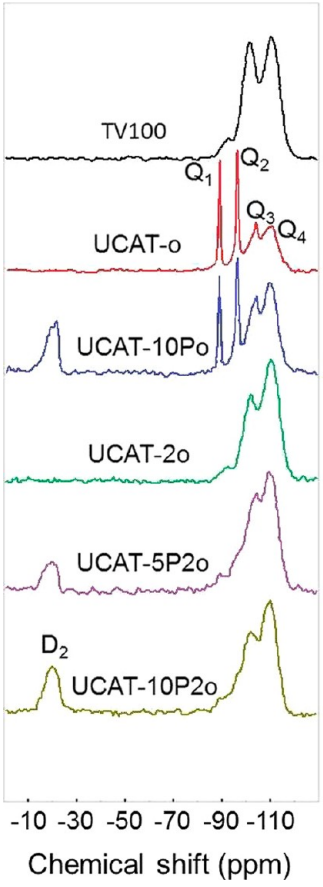

Figure 10. ^{29}Si NMR spectra for the nanomaterials under study.

Differences according to the *n*-octylamine content were also observed between the spectra of the UCA materials. The two spectra from the xerogels containing the lowest proportion of n-octylamine (UCAT-o and UCAT-10Po) presented Q_1 (−89 ppm) and Q_2 (−91 ppm) units in conjunction with Q_3 and Q_4 species, which indicated that the silica is not completely condensed and subsequently, some ethoxy groups could be present in the material.[35] In the case of xerogels with the highest octylamine content (UCAT-2o, UCAT-5P2o, and UCAT-10P2o), the signals from Q_1 and Q_2 are either absent or observed as a weak 'shoulder'. This finding confirms the role played by the n-octylamine as catalyst during the sol–gel transition.

In the nanomaterials containing PDMS, the spectra showed D_2 species characterized by a broad peak, around −15 ppm. Their intensity is greater when the PDMS content is higher. As Babonneau has previously discussed,[34] this broad component could be due to PDMS chains in a constrained environment, corresponding to crosslinking points with silica particles. These results corroborate the structure models presented in Figures 6 and 8, showing a hybrid material in which PDMS chains create bridges linking the silica particles.

Effectiveness on a Building Stone. The materials synthesized in this study with the highest n-octylamine content were sprayed, under laboratory conditions, onto a biocalcareous building stone in order to investigate their effectiveness as a consolidant for restoration purposes. In addition, we also investigated their effectiveness as a hydrophobic product on the same stone. The two commercial products under study were also tested. Uptake of the UCA products (ranging from 8 to 9% w/w) was slightly higher than that corresponding to the TV100 and BS290 products (7 and 4% w/w, respectively). The dried matter values obtained were similar for UCA materials and the TV100 product (around 4% w/w) whereas BS290 dry matter was significantly lower (0.25% w/w), its evaporated mass being around 85%. This finding demonstrates that the BS290 solvent is completely removed during drying on the stone. As previously discussed, this product does not penetrate into the pore structure of the stone; it only creates a thin film on the stone surface. Thus, BS290 cannot act to consolidate the stone pore structure.

The effect of the products on the mechanical robustness of the stone under study was evaluated by measuring the drilling resistance of each of the treated stones and their untreated counterpart. Drilling resistance vs. testing depth profiles are shown in Figure 11. As Delgado–Rodrigues et al. reported,[36] this technique has a very high discriminating power for evaluating the effectiveness of consolidant products on stone. The commercial product had almost no consolidant effect on the stone, whereas the stone samples treated with three UCA products significantly increased the mechanical resistance of the stone treated. In particular, the stone treated with the UCA product without PDMS showed the highest increase (by a factor of 5). Moreover, this increase was evident across the full

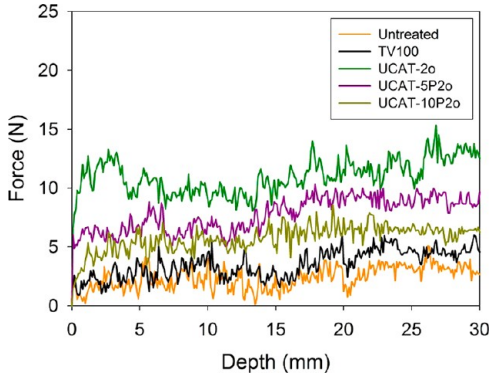

Figure 11. Drilling resistance versus testing depth of treated stones and their untreated counterpart.

dx.doi.org/10.1021/am300964q | ACS Appl. Mater. Interfaces 2012, 4, 4259–4269

depth of stone tested (30 mm), demonstrating that the UCA product efficiently penetrated into the stone pore structure.

Figure 12 shows water droplet static contact angle (CA) values and their corresponding advancing and receding CA values for the surfaces of stone samples treated with the products under study. All the products evaluated increased the CA value obtained for the untreated stone specimens (36° ± 3). As expected, the samples with TV100 did not present hydrophobic properties whereas the stone treated with BS290 (containing organic groups) did show hydrophobic behavior.

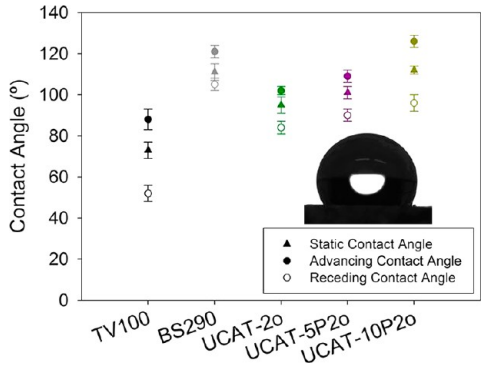

Figure 12. Static CA values and their corresponding advancing and receding CA for the stones treated. Image included corresponds to a droplet on stone treated with UCAT-10P2o.

With regard to the UCA products, the stones treated with the hybrid gels (UCAT-5P2o and UCAT-10P2o) presented higher CA values than the samples treated with UCAT-2o, because of the presence of PDMS chains integrated into the silica skeleton of the material.[6] It is well known that PDMS has a very low surface energy, which produces contact angles in the range of 95−115°,[37] as observed for the stone surfaces treated with the hybrid products in this study. Moreover, higher PDMS content produces higher CA values. Finally, we associate the anomalous high CA value obtained for stones treated with the UCAT-2o product (without PDMS) to the efficient penetration of the product into the pore structure of stone, which prevents water absorption into the stone pores.

The relatively high hysteresis (difference between receding and advancing CA) observed in all the UCA products could be associated with the roughness produced by these products on the stone surface. As observed by AFM (Figure 7), the shrinkage of PDMS chains during drying produces roughness peaks creating grooves in which the water droplets are pinned.[38] Because of the low PDMS content (10% v/v), the product is not capable of producing a surface texture with continuous PDMS peak roughness in which the droplets could move without a kinetic barrier, minimizing hysteresis, as we demonstrated previously for products with higher PDMS content.[6]

Because all the products containing organic components (UCAT-5P2o, UCAT-10P2o, and BS290) presented receding CA values higher than 90°, all these products could be theoretically capable of preventing the penetration of water into the stone.[39] We checked this claim by performing a test of water absorption by capillarity (WAC) on stone samples treated with these products. The water absorbed mass values were 10 and 4% w/w for the untreated specimens and their counterparts treated with the commercial product TV100, respectively. In the case of the stones treated with all the UCA products and BS290 products, the water absorbed mass values were below 0.5% w/w, demonstrating the hydrophobic effectiveness of the products under study.

From the results obtained, we conclude that the solvent-free nanomaterials synthesized in our laboratory in the presence of n-octylamine are effective as both consolidants and hydrophobic products. We have also demonstrated that they are produced, in situ, on the substrate. They can therefore be applied on the exterior of buildings or on other outdoor materials for restoration and conservation purposes. These new nanomaterials will become available as commercial products under an exploitation patent.[40]

CONCLUSIONS

We have developed a novel volatile organic component-free synthesis for producing nanomaterials. Particularly, these materials are capable of increasing the mechanical resistance of building substrates. It is a simple and low-cost procedure in which a silica oligomer is mixed with a surfactant by ultrasonic agitation. We also obtained similar nanomaterials with additional hydrophobic properties simply by adding an organic component, PDMS, to the starting sol. The surfactant serves as an agent that directs the pore structure of the materials, preventing cracking during drying. Because calcination or other additional processes are not required as part of the synthesis, materials produced by this route can be applied onto exposed outdoor substrates of building stone, including facades, floors and other elements. We also characterized the structure of the two types of nanomaterial synthesized, demonstrating that the surfactant creates a mesostructure consisting of a particular configuration of silica particles. We also discuss how PDMS chains act as bridges linking the silica particles. Finally, we have demonstrated the consolidant and hydrophobic effectiveness of these products on a common building stone, being more effective than the commercial product evaluated.

ASSOCIATED CONTENT

Supporting Information

The FTIR spectra of the commercial products TES40 and PDMS and ^{13}C NMR spectrum of UCA gel with the highest *n*-octylamine content. This material is available free of charge via the Internet at http://pubs.acs.org.

AUTHOR INFORMATION

Corresponding Author

*E-mail: mariajesus.mosquera@uca.es. Fax: +34-956016471. Tel: +34-956016331.

Notes

The authors declare no competing financial interest.

ACKNOWLEDGMENTS

We are grateful to the Spanish Government and the European Regional Development Fund (ERDF) for financial support under research projects MAT2010-16206 and REGENERA (Innpacto subprogramme). We also thank the Regional Government of Andalusia for its support under the projects TEP2092, TEP6386 and TEP-243 group. J.F.I. is grateful for his pre-doctoral grant associated with the TEP2092 project. The authors also want to thank to the Bahía San Cristobal quarry and its manager D. Manuel Muñoz for supplying the stone samples.

REFERENCES

(1) Scherer, G.W. *J. Am. Ceram. Soc.* **1990**, *73*, 3−14.
(2) Mosquera, M.J.; de los Santos, D.M.; Rivas, T.; Sanmartín, P.; Silva, B. *J. Nano Res.* **2009**, *8*, 1−12.
(3) Mosquera, M.J.; de los Santos, D.M.; Montes, A.; Valdez-Castro, L. *Langmuir* **2008**, *24*, 2772−2778.
(4) Mosquera, M.J.; de los Santos, D.M; Rivas, T. *Langmuir* **2010**, *26*, 6737−6745.
(5) Mosquera, M.J.; de los Santos, D.M.; Valdez-Castro, L.; Esquivias, L. *J. Non-Cryst. Solids* **2008**, *354*, 645−650.
(6) Illescas, J.F.; Mosquera, M.J. *J. Phys. Chem. C* **2011**, *115*, 14624−14634.
(7) Pinho, L.; Mosquera, M.J. *J. Phys. Chem. C* **2011**, *115*, 22851−22862.
(8) Simionescu, B.; Olaru, M.; Aflori, M.; Cotofana, C. *High Perform. Poly.* **2010**, *22*, 42−55.
(9) Xu, F.; Li, D; Zhang, H.; Peng, W. *J. Sol−Gel Sci. Technol.* **2012**, *61*, 429−435.
(10) Tanev, P.T.; Pinnavaia, T.J. *Science* **1995**, *267*, 865−867.
(11) Tanev, P.T.; Pinnavaia, T.J. *Chem. Mater.* **1996**, *8*, 2068−2079.
(12) Mercier, L.; Pinnavaia, T.J. *Chem. Mater.* **2000**, *12*, 188−196.
(13) Mirgorodskaya, A.B.; Kudryavtseva, L.A.; Zuev, Y.F.; Archipov, V.P.; Idyllatullin, Z. Sh. *Mendeleev Commun.* **1999**, *9*, 196−198.
(14) UNE-EN 1925. *Natural Stone Test Methods. Determination of Water Absorption Coefficient by Capillarity*; AENOR: Madrid, Spain, 1999.
(15) Mrowetz, M.; Balcerski, W.; Colussi, A.J.; Hoffmann, M.R. *J. Phys. Chem. B* **2004**, *108*, 17269−17272.
(16) Han, A.J.; Guo, J.; Yu, H.; Zeng, Y.; Huang, Y.F.; He, H.Y; Long, Y.C. *ChemPhysChem* **2006**, *7*, 607−613.
(17) Ion, A.; Van Doorslaer, C.; Parvulescu, V.; Jacobs, P.; De Vos, D. *Green Chem.* **2008**, *10*, 111−116.
(18) Mckenzie, J.D.; Chung, Y.J.; Hu, Y. *J. Non-Cryst. Solids* **1992**, *147&148*, 271−279.
(19) Kruk, M.; Jaroniec, M. *Chem. Mater.* **2001**, *13*, 3169−3183.
(20) Kruk, M.; Jaroniec, M.; Sayari, A. *Langmuir* **1997**, *13*, 6267−6273.
(21) Barret, E.P.; Joyner, L.G.; Halenda, P.P. *J. Am. Chem. Soc.* **1951**, *73*, 373−380.
(22) Orcel, G.; Hench, L.L.; Artaki, I.; Jonas, J.; Zerda, T.W. *J. Non-Cryst. Solids* **1988**, *105*, 223−231.
(23) Bogush, G.H.; Zukoski, C.F., IV *J. Colloid Interface Sci.* **1991**, *142*, 1−18.
(24) Bogush, G.H.; Zukoski, C.F., IV *J. Colloid Interface Sci.* **1991**, *142*, 19−34.
(25) Kosuge, K.; Singh, P.S. *Microporous Mesoporous Mater.* **2001**, *44-45*, 139−145.
(26) Zhang, X.; Ye, H.; Xiao, B.; Yan, L.; Lv, H; Jiang, B. *J. Phys. Chem. C* **2010**, *114*, 19979−19983.
(27) Rodrigues, D.E.; Rennan, A.B.; Betrabet, C.; Wang, B.; Wilkes, G.L. *Chem. Mater.* **1992**, *4*, 1437−1446.
(28) Tellez, L.; Rubio, J.; Rubio, F.; Morales, E.; Oteo, J.L. *J. Mater. Sci.* **2003**, *38*, 1773−1780.
(29) Demjén, Z.; Pukánsky, B.; Földes, E.; Nagy, J. *J. Colloid Interface Sci.* **1997**, *190*, 427−436.
(30) Prado, A.G.S.; Airoldi, C. *J. Mater. Chem.* **2002**, *12*, 3823−3826.
(31) Weigel, C.H.; Kellner, R. *Fresenius Z. Anal. Chem.* **1989**, *335*, 663−668.
(32) Sekine, M.; Katayama, S.; Mitomo, M. *J. Non-Cryst. Solids* **1991**, *134*, 199−207.
(33) Innocenzi, P. *J. Non-Cryst. Solids* **2003**, *316*, 309−319.
(34) Babonneau, F. *Polyhedron* **1994**, *13*, 1123−1130.
(35) Noble, K.; Seddon, A.B.; Turner, M.L.; Chevalier, P.; Mackinnon, I.A. *J. Sol−Gel Sci. Technol.* **2000**, *19*, 807−810.
(36) Delgado Rodrigues, J.; Ferreira Pinto, A.; Rodrigues da Costa, D. *J. Cult. Herit.* **2002**, *3*, 117−125.
(37) Wu, Y.L.; Chen, Z.; Zeng, X.T. *Appl. Surf. Sci.* **2008**, *254*, 6952−6958.
(38) Gao, L.; McCarthy, T.J. *Langmuir* **2009**, *25*, 14105−14115.
(39) Della Volpe, C.; Penati, A.; Peruzzi, R.; Siboni, S.; Toniolo, L.; Colombo, C. *J. Adhesion Sci. Technol.* **2000**, *14*, 273−299.
(40) Mosquera, M.J.; Illescas, J.F.; Facio, D.S. Spanish Patent. No. P201200152, February 16, 2012.